

Synthesis, characterization and photocatalytic activity of Zn²⁺, Mn²⁺ and Co²⁺ doped SnO₂ nanoparticles

Oeindrila Mukhopadhyay¹, Soumita Dhole¹, Badal Kumar Mandal^{1,*}, Fazlur-Rahman Nawaz Khan², Yong-Chien Ling^{3,**}

¹Trace Elements Speciation Research Laboratory, Department of Chemistry, School of Advanced Sciences, Vellore Institute of Technology, Vellore-632014; ²Organic and Medicinal Chemistry Research Laboratory, Department of Chemistry, School of Advanced Sciences, Vellore Institute of Technology, Vellore-632014, Tamil Nadu, India; ³Department of Chemistry, National Tsing Hua University, Hsinchu 30013, Taiwan

*corresponding author e-mail address: badalmandal@vit.ac.in; ycling@mx.nthu.edu.tw

ABSTRACT

Nanomaterials with many improved properties have been used in versatile applications. Herein we have synthesized SnO₂ NPs doped with transition metal ions such as Zn²⁺, Mn²⁺ and Co²⁺ through a facile and inexpensive hydrothermal approach. The synthesized nanomaterials were characterized by XRD, FT-IR, SEM and UV-Vis analysis. The optical properties of the NPs were characterized by using UV-vis and photoluminescence spectroscopy (PLS). Their photocatalytic performances were investigated by degrading methylene blue (MB) dye with UV irradiation. Transition metal doping to SnO₂ NPs improved the photocatalytic activity to degradation of methylene blue dye due to tuning of band gap energy i.e. lowering of band gap energy compared to undoped SnO₂ NPs. The results suggest that the synthesized NPs could be used efficiently for remediation/degradation of environmentally hazardous dyes from waste water or environmental cleanup.

Keywords: Metal doped SnO₂ nanoparticles, methylene blue dye, photoluminescence, UV irradiation.

1. INTRODUCTION

Luxurious lifestyle of humans has brought many unwanted changes in our mother environment which challenges the ecology of earth natural systems resulting in many environmental problems. So it is a very important and urgent challenge to find proper semiconducting material which can produce H₂ and O₂ through a photocatalytic reaction. TiO₂ NPs was discovered in 1972 and is one of the best photocatalysts among the semiconducting metal oxides nanoparticles [1-6]. Rutile structured SnO₂ NPs was studied extensively after TiO₂ NPs because SnO₂ NPs possess high surface area and temperature resistance, low toxicity and high ability does redox reactions with gases [7]. In addition, SnO₂ NPs are n-type semiconducting materials with a band gap of 3.6 eV at 330K with an exciton Bohr radius of 2.7nm [8,9]. Recently Li et al. (2017) used ZnO nanowires doped with Mn²⁺ and Co²⁺ ions to improve its visible-light absorption for photocatalytic degradation of methyl orange (MO) dye [7]. Etacheri et al. (2012) used Mg-doped ZnO NPs for efficient Sunlight drove photocatalysis study [10]. Similarly, Mohamed and Shawky (2018) reported the synthesis of Mn-doped ZnO nanoparticles on CNT support and used for photocatalytic degradation of malachite green dye under visible light [11]. Babu et al. (2017) used Cu²⁺-doped SnO₂ quantum dots (QDs) for higher photocatalytic activity compared to pure SnO₂ QDs [12]. Zhang et al. (2017) synthesized novel TiO₂/Ag/SnO₂ composites photocatalyst for photodegradation of methylene blue (MB) via visible light and found significantly enhanced 9.5 times catalytic activity compared to individual TiO₂ or the binary composite (TiO₂/Ag or TiO₂/SnO₂) [13]. Zeferino et al. (2019) used indium doped SnO₂ NPs for UV degradation of MB dye and reported that there was no intermediate formation i.e. direct mineralization

during photodegradation compared to the production of intermediate byproducts such as azure A, azure B, and azure C by pure SnO₂ NPs [14].

PrabhakarVattikuti et al. (2018) prepared SnO₂-ZnO QDs/g-C₃N₄ hybrid for the degradation of pollutants and hydrogen gas (H₂) generation under visible-light irradiation. Also, the synergistic effect of doped oxides increased visible light absorption of the hybrid which enhanced its photoelectrochemical activity as a promising electrode material [15]. Zhang et al. (2011) prepared SnS₂/SnO₂ nanocomposites with tunable SnO₂ contents and observed superior photocatalytic activity compare to both SnS₂ NPs and physically mixed SnS₂/SnO₂ composite NPs [16]. Yin et al. (2014) synthesized SnO₂/g-C₃N₄ nanocomposite visible light sensitive photocatalysts for methyl orange (MO) degradation under visible light exposure (wavelength ≥400 nm) and found much higher efficiency than that of pure g-C₃N₄ [17]. Gao et al. (2018) developed visible light sensitive photocatalyst g-C₃N₄/SnO₂:Sb composites by a facile hydrothermal method and tested for degradation of rhodamine B. The test results showed the superior photocatalytic efficiency of g-C₃N₄/SnO₂:Sb composites compare to g-C₃N₄/SnO₂ without doping Sb [18] suggesting promising materials for the potential application in environmental protection. Jiang et al. (2019) prepared yttrium-doped TiO₂ hollow spheres (Y-TiO₂HS) via a sol-gel method. The as-synthesized materials showed higher thermal stability with Y-doping and enhanced photocatalytic activity of TiO₂ by 3 times compare to un-doped TiO₂HS [19].

Although different methods have been used to synthesize SnO₂ NPs such as sol gel [20], microemulsion [21], hydrothermal [22], co-precipitation [23], chemical precipitation [24] and polyol [25],

all of them use toxic and hazardous chemicals and solvents which are not friendly to humans and environment. Hence it is urgently necessary to find novel and environmentally friendly materials synthesizing by eco-friendly methods for different applications [26-28].

Less toxic semiconductor rutile SnO₂ NPs has high surface area, temperature resistance and sensitivity in reducing environmental

pollutants. Among available photocatalysts, n-type semiconducting SnO₂ (wide direct bandgap of about 3.6eV) is highly efficient in degrading water pollutants [1]. Hence the main objective of the present study was to synthesize novel Zn²⁺, Mn²⁺ and Co²⁺ ions doped SnO₂ NPs for environmental cleanup, especially degradation of organic toxic methylene blue (MB) dye under UV irradiation.

2. MATERIALS AND METHODS

2.1. Materials.

All analytical grade reagents SnCl₂.2H₂O, Co(OAC)₂, Mn(OAC)₂ and Zn(OAC)₂ were purchased from Sigma Aldrich (Bangalore) and Milli-Q water was used for the synthesis of nanomaterials by hydrothermal method, degradation of methylene blue dye (Fig. 1) and other studies.

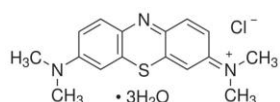


Figure 1. Structure of Methylene Blue (MB) dye.

3. RESULTS

3.1. X-Ray diffraction studies.

Normally X-ray diffraction (XRD) studies are done to find out the crystallinity and phase purity of the synthesized nanomaterials. Sometimes it is used to determine crystallite size of the particles. Initially, a few milligrams of the sample was dispersed in distilled water with sonication and then one or two drops of the dispersion was placed on the copper-grid followed by solvent evaporation for XRD analysis. The XRD patterns of SnO₂NPs, Zn-doped SnO₂NPs, Mn-doped SnO₂NPs and Co-doped SnO₂NPs are shown in Fig. 2-3. The XRD pattern was identified by comparing with the JCPDdata card No. 96-100-0063. The XRD patterns of Zn-doped (blue), Mn-doped (red) and Co-doped (grey) SnO₂ nanoparticles had the same diffraction peaks as SnO₂. There were no other sharp peaks to be attributed to zinc, manganese or cobalt elements in the XRD patterns which indicate that doped Zn²⁺, Mn²⁺ and Co²⁺ ions had no effect on crystalline structure of SnO₂.

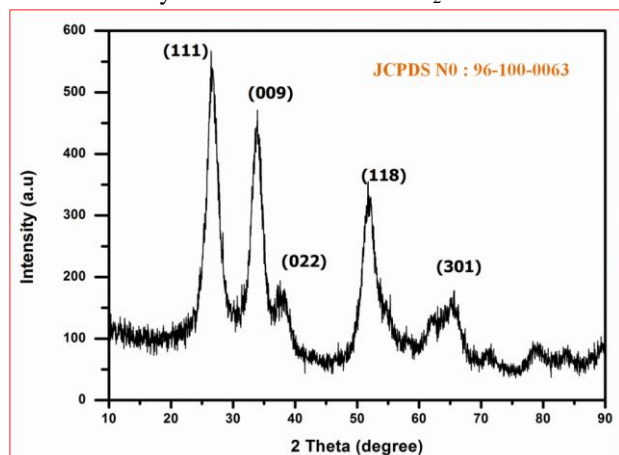


Figure 2. XRD pattern of pure SnO₂ NPs.

2.2. Synthesis of SnO₂ NPs & Zn²⁺, Mn²⁺ and Co²⁺ doped SnO₂ NPs.

200 mL precursor solution (0.075 M) was prepared by mixing stannous chloride dehydrate and manganese(or cobalt or zinc) acetate dehydrate at the molar ratio of 9:1 in deionized water. Then pH of the solution was adjusted to 10 with ammonia at room temperature by stirring for half an hour. Finally, the as-prepared substrate solutions were kept in a Teflon-lined autoclave and heated at 90⁰C for 6 h followed by washing with water and drying at room temperature. The same procedure was followed in synthesizing SnO₂ NPs without other precursor solutions.

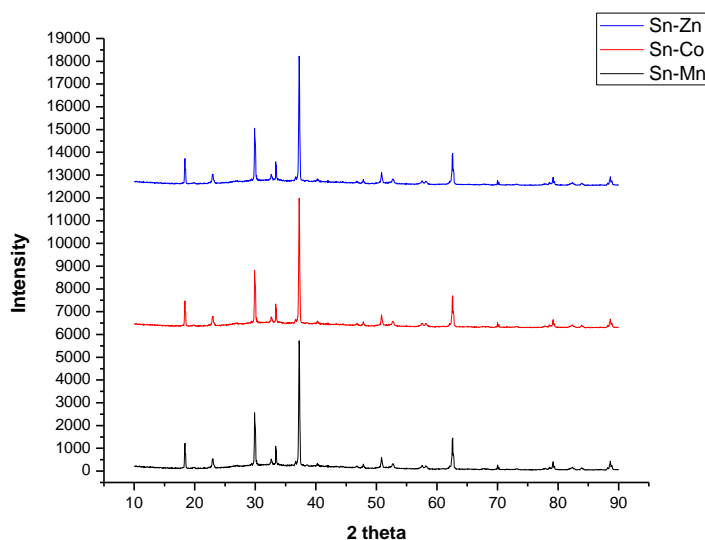


Figure 3. XRD patterns of Zn-doped SnO₂ NPs (blue), Co-doped SnO₂ NPs (red) and Mn-doped SnO₂ NPs (grey).

3.2 FT-IR Studies.

FT-IR analysis is done to detect any functional groups present on the surface of nanomaterials or metal oxide formation.

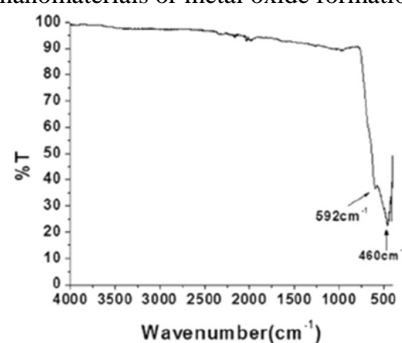


Figure 4. FT-IR spectrum of pure SnO₂ NPs.

The FT-IR spectrum of the synthesized pure SnO₂NPs is shown in Fig. 4 while that of SnO₂ NPs doped with Zn²⁺ (black), doped with Mn²⁺(blue) and doped with Co²⁺ (red) shows two representative bands (Fig. 5). The band at around 590 cm⁻¹ develops due to Sn-O-Sn anti-symmetric vibration and at 460 cm⁻¹for Sn-O symmetric vibration while band around 3200cm⁻¹ is due to the doping of transition metal. This information confirm the formation of metal oxide bond.

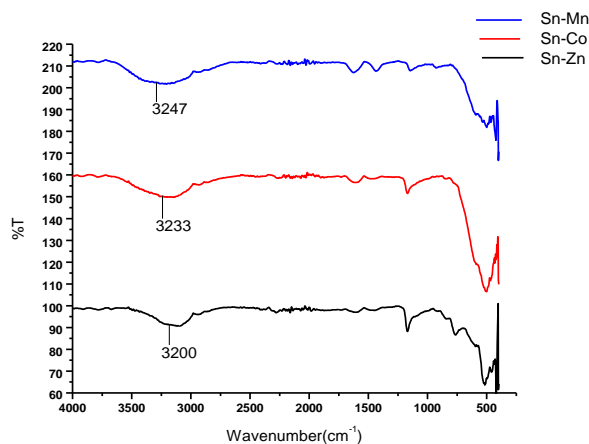


Figure 5. FT-IR spectra of Mn-doped SnO₂ NPs (blue), Co-doped SnO₂ NPs (red) and Zn-doped SnO₂ NPs (black).

3.3. UV-Vis and Photoluminescence studies.

Many parameters influence the optical properties of semiconductor materials. In general, energy gap is the critical one which influences the most in photocatalytic activities. Also, impurity centers and surface roughness tunes its efficiency. In addition, oxygen vacancies can enhance the formation of electron-hole pairs. UV-vis spectrophotometry was used to check its optical properties.

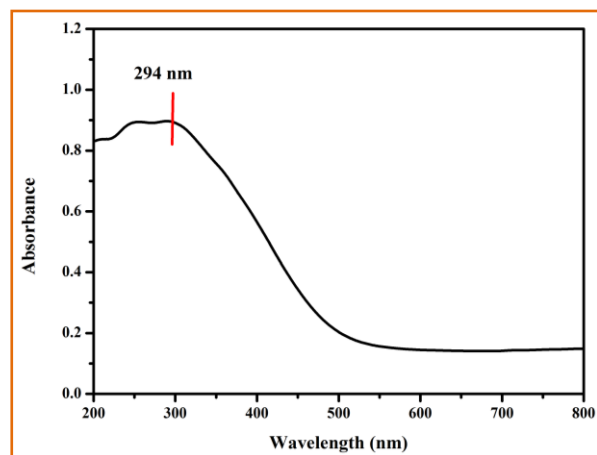


Figure 6. UV-Visible spectrum of pure SnO₂ NPs.

Undoped SnO₂ NPs showed maximum absorbance at 294 nm in UV region (Fig. 6). Figure 7 shows the absorption bands at 249 nm for Mn-doped SnO₂ NPs (blue), 261 nm for Co-doped SnO₂ NPs (red) and 269 nm for Zn-doped SnO₂ NPs (black) respectively. There is a clear blue shift on doping of metal ions on SnO₂ NPs (Fig. 7). Figure 8 shows an emission band at 348 nm in photoluminescence spectrum (PLS) of the synthesized undoped SnO₂ NPs. It suggests that oxygen or other interstitial defects in the crystals may cause this fluorescence response. Figure 9 shows photoluminescence emission band at 249 nm for Mn-doped SnO₂

NPs (blue), 261 nm for Co-doped SnO₂ NPs (red) and 269 nm for Zn-doped SnO₂ NPs (black).

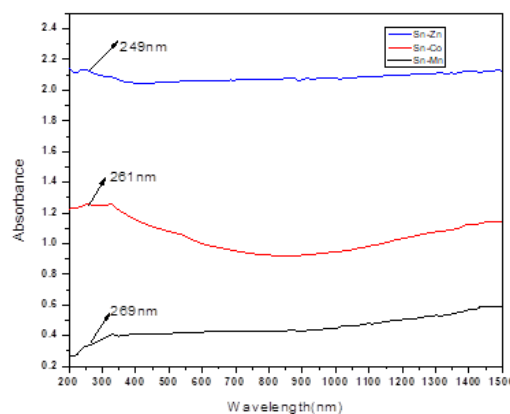


Figure 7. UV-Vis absorption spectra of Zn-doped SnO₂ NPs (blue), Co-doped SnO₂ NPs (red) and Mn-doped SnO₂ NPs (black).

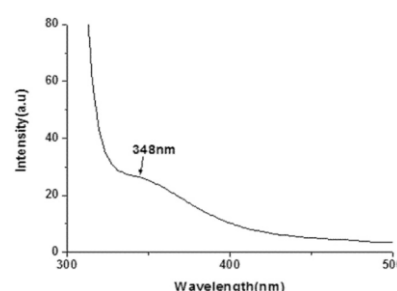


Figure 8. Photoluminescence (PL) spectrum of undoped SnO₂ NPs.

Photoluminescence (PL) is influenced by degree of recombination of the electron-hole pairs which are directly proportional. The PL intensities of doped SnO₂ NPs are lower than that of pure SnO₂ NPs, demonstrating higher fluorescence activity of doped SnO₂ NPs due to trapping of electrons by doped metal ions which suppress the recombination of electron-hole pairs. It is obvious that doped SnO₂ NPs had better optical properties with lower recombination rate.

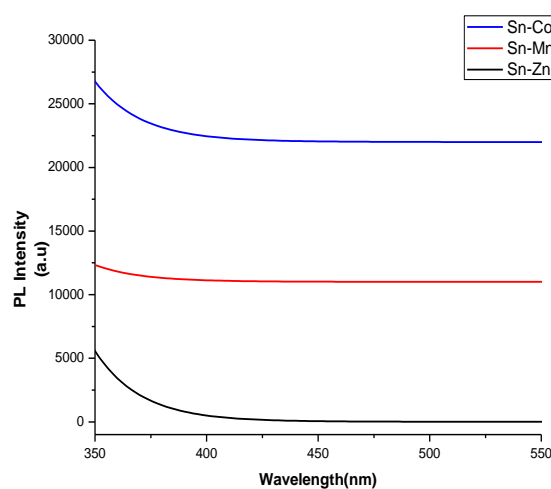


Figure 9. Photoluminescence (PL) spectra of Zn-doped SnO₂ NPs (blue), Co-doped SnO₂ NPs (red) and Mn-doped SnO₂ NPs (black).

3.4. SEM Studies.

SEM analysis was carried out to see the size and shape i.e. morphology and elemental analysis of the synthesized nanomaterials after proper sample preparation. Figure 10 shows

SEM micrographs of Co-doped SnO₂ NPs (Fig. 10a-b), Mn-doped SnO₂ NPs (Fig. 10c-d) and Co-doped SnO₂ NPs (Fig. 10e-f), which documents the shape and morphology of the NPs.

Band gap calculation.

Interstitial defects in SnO₂ NPs crystal system increases the energy gap of 3.6 eV as well as generates new energy levels lowering energy gap i.e. band gap. In the present study a lower energy gap value from 3.6 to 2.5-1.2 eV is observed (Fig. 11).

The band gap energy (E_g) is estimated using the following equation as $(\alpha h\nu)^2 = A(h\nu - E_g)^n$, where α = Absorption coefficient, A is a constant and $n=2$ for direct and $n=1/2$ for indirect transition. An extrapolation of Tauc plot of ' $h\nu$ ' versus ' $(\alpha h\nu)^2$ ' gives optical energy gap (E_g) value as shown in Fig. 11.

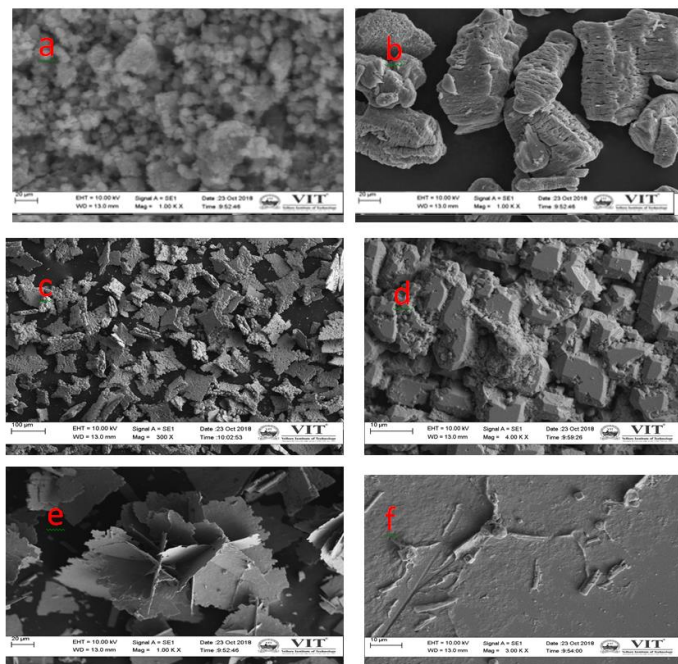


Figure 10. SEM micrographs of pure SnO₂ NPs (a), Mn-doped SnO₂ NPs (b), Co-doped SnO₂ NPs (c, d) and Zn-doped SnO₂ NPs (e, d).

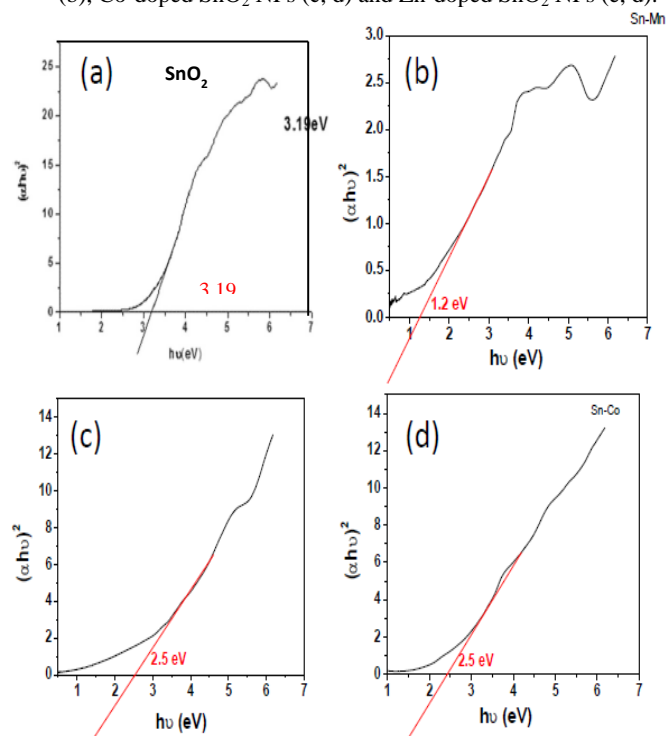


Figure 11. Tauc plots for undoped SnO₂ NPs (a), Mn-doped SnO₂ NPs (b), Zn-doped SnO₂ NPs (c) and Co-doped SnO₂ NPs (d).

The results show that band gap energy of undoped SnO₂ NPs is 3.19 eV, but that of Mn-doped, Zn-doped and Co-doped SnO₂ NPs are 1.2 eV, 2.5 eV and 2.5 eV respectively. It clearly demonstrates that Mn-doped SnO₂ NPs possess lower band gap energy (E_g=1.2 eV) than others and it may not be good photocatalyst due to higher possibility of recombination of photogenerated electron-hole pairs. Practically, Zn-doped and Co-doped SnO₂ NPs degraded completely MB dyes within 45 min compared to 75 min for Mn-doped and 120 min for undoped SnO₂ NPs.

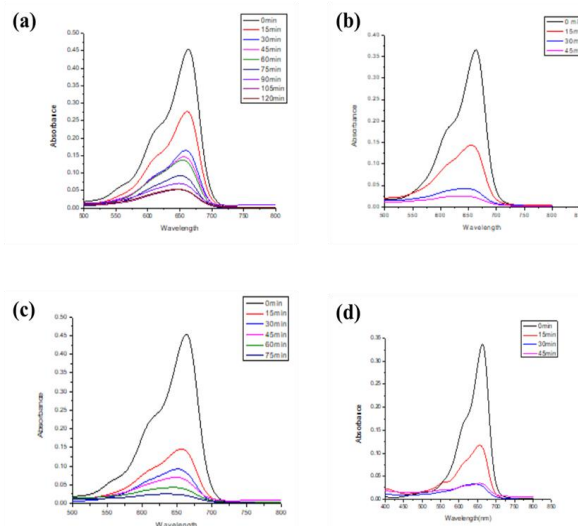


Figure 12. Photodegradation of MB dye (10 mg/L) by undoped SnO₂ NPs (a), Zn-doped SnO₂ NPs (b), Mn-doped SnO₂ NPs (c) and Co-doped SnO₂ NPs (d).

3.5. Photocatalytic Activity Study.

Degradation of MB dye was checked under 125W UV lamp (Hg lamp, λ_{max} 254 nm) by undoped and doped photocatalyst SnO₂ NPs. 60 mL MB dye (20 mg L⁻¹) with 20 mg of catalyst at room temperature. The samples were collected for every 15 min time interval and centrifuged before analysis. Up to 45 min of exposure colour intensity was checked using UV-vis spectrophotometer at 552 nm. One blank experiment without catalyst was done under identical conditions as reference sample (Fig. 12) and no absorbance intensity of MB dye solution was seen at 552 nm after one hour (data not shown) was seen.

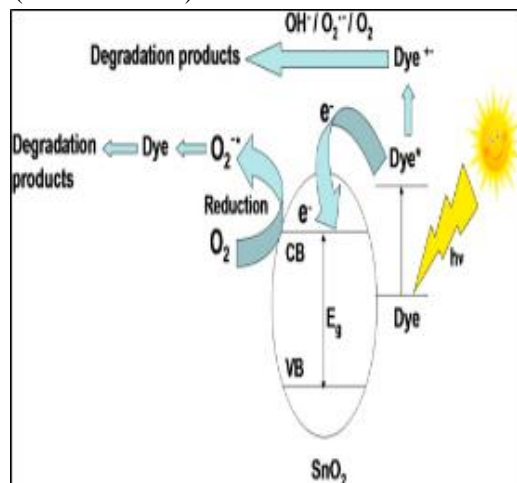


Figure 13. Mechanistic pathways of MB dye photodegradation by using undoped and transition metal-doped SnO₂ NPs.

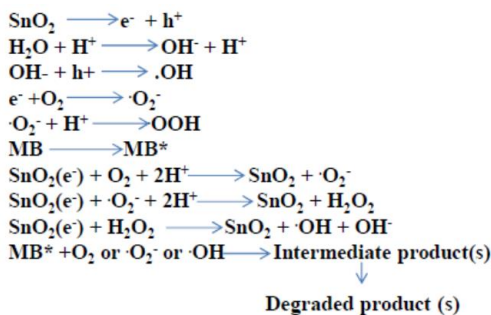


Figure 14. Generation of ROS and Degradation pathways of MB dye in the presence of transition metal doped SnO₂ NPs.

On exposure of UV light (λ_{max} 254 nm) electrons of SnO₂ NPs get excited to the conduction band creating a hole in the valence band. Afterwards electrons in conduction band react with O₂ to form super oxide and the hole in valence band react with H₂O to form OH[·] ions i.e. free radicals and super oxide ($\cdot\text{OH}$, $\cdot\text{O}_2^-$). The generated ROS are the oxidizing agents, which oxidizes the dye (Fig. 13). The possible degradation mechanism of dye with catalyst by 254 nm UV irradiation is described schematically in Fig. 12. The stepwise chemical equations followed by degradation of MB by *in situ* generations of ROS such as $\cdot\text{OOH}$, $\cdot\text{OH}$ and $\cdot\text{O}_2^-$ (Fig. 14) [29].

4. CONCLUSIONS

In the present study, we have prepared SnO₂ NPs and SnO₂ NPs doped with Zn, Mn & Co successfully and is characterized by XRD, FT-IR, SEM, UV-Visible and photoluminescence studies. The obtained doped NPs showed the band gap around 2.5 eV which is lesser than the undoped SnO₂ NPs (~ 3.6 eV). We have studied the photocatalytic activity of both undoped and doped SnO₂ NPs with respect to time. Further we have studied the effect

5. REFERENCES

- Fujishima, A.; Honda, K. Electrochemical photolysis of water at a semiconductor electrode. *Nature* **1972**, *238*, 37–38, <https://doi.org/10.1038/238037a0>.
- Yan, S.C.; Li, Z.S.; Zou, Z.G. Photodegradation of Rhodamine B and Methyl Orange over Boron-Doped Cd₃N₄ under Visible Light Irradiation. *Langmuir* **2010**, *26*, 3894–3901, <https://doi.org/10.1021/la904023j>.
- Li, Z.C.; Xiong, S.; Wang, G.J.; Xie, Z.; Zhang, Z.J. Role of Ag₂S coupling on enhancing the visible-light induced catalytic property of TiO₂ nanorod arrays. *Sci. Rep.* **2016**, *6*, 19754, <https://doi.org/10.1038/srep19754>.
- Chen, C.H.; Li, Z.C.; Lin, H.N.; Wang, G.J.; Liao, J.C.; Li, M.Y.; Lv, S.S.; Li, W. Enhanced visible light photocatalytic performance of ZnO nanowires integrated with CdS and Ag₂S. *Dalton Trans.* **2016**, *45*, 3750–3758, <http://dx.doi.org/10.1039/C5DT04533A>.
- Li, Z.C.; Teng, Y.; Chen, C.H.; Lv, S.S.; Wang, G.J.; Zhang, Z.J. Effect of Xe ion irradiation on photocatalytic performance of oblique TiO₂ nanowire arrays. *Appl. Surf. Sci.* **2015**, *327*, 478–482, <https://doi.org/10.1016/j.apsusc.2014.12.009>.
- Li, Q.; Guo, B.D.; Yu, J.G.; Ran, J.R.; Zhang, B.H.; Yan, H.J.; Gong, J.R. Highly Efficient Visible-Light-Driven Photocatalytic Hydrogen Production of CdS-Cluster-Decorated Graphene Nanosheets. *J. Am. Chem. Soc.* **2011**, *133*, 10878–10884, <https://doi.org/10.1021/ja2025454>.
- Li, W.; Wang, G.; Chen, C.; Liao, J.; Li, Z. Enhanced Visible Light Photocatalytic Activity of ZnO Nanowires Doped with Mn²⁺ and Co²⁺ Ions. *Nanomaterials* **2017**, *7*, 20, <https://doi.org/10.3390/nano7010020>.

Also, the rate of photodegradation of MB dye was checked with varying doses of catalyst (5, 10, 20 mg) and the degradation kinetics increased with the increasing dose of catalyst (Fig. 15a) i.e. the time of degradation decreased from 70 min to 40 min.

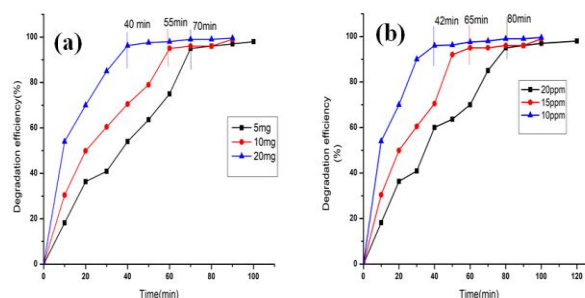


Figure 15. Photodegradation of MB dye: (a) effect of catalyst dosage (5–20 mg) on MB dye (10 mg/L) and (b) effect of dye concentrations (10–20 mg/L) at a catalyst dose of 10 mg.

Similarly, the rate of photodegradation was checked with varying concentrations of MB dye (10, 15, 20 mg/L) at a constant catalyst dose of 20 mg and the rate of degradation decreased with increasing dye doses from 10 mg/L to 20 mg/L i.e. the time of degradation increased from 42 min to 80 min (Fig. 15b).

of catalytic doses and the effect of dye concentration on the photodegradation of MB dye. These doped SnO₂ NPs could be promising photocatalyst in degrading textile dyes compared to undoped SnO₂ NPs in the coming days and would solve demanding environmental pollution caused by industrial activities, namely textile industries throughout India and abroad.

- Cao, H.; Qiu, X.; Liang, Y.; Zhang, L.; Zhao, M.; Zhu, Q. Sol-Gel template synthesis and photoluminescence of n-type and p-type semiconductor oxide nanowires. *Chem. Phys. Chem.* **2006**, *7*, 497–501, <https://doi.org/10.1002/cphc.200500452>.
- Lee, E.J.H.; Ribeiro, C.; Giraldo, T.R.; Longo, E.; Leite, E.R.; Varela, J.A. Photoluminescence in quantum-confined nanocrystals: evidence of free exciton decay. *Appl. Phys. Lett.* **2004**, *84*, 1745–1747, <https://doi.org/10.1063/1.1655693>.
- Etacheri, V.; Roshanand, R.; Kumar, V. Mg-Doped ZnO Nanoparticles for Efficient Sunlight-Driven Photocatalysis. *ACS Appl. Mater. Interfaces*, **2012**, *45*, 2717–2725, <https://doi.org/10.1021/am300359h>.
- Mohamed, R.M.; Ahmed, S. CNT supported Mn-doped ZnO nanoparticles: simple synthesis and improved photocatalytic activity for degradation of malachite green dye under visible light. *Applied Nanoscience* **2018**, *8*, 1179–1188, <http://dx.doi.org/10.1007/s13204-018-0742-8>.
- Babu, B.; Kadam, A.N.; Ravikumar, R.V.S.S.N.; Byon, C. Enhanced visible light photocatalytic activity of Cu-doped SnO₂ quantum dots by solution combustion synthesis. *J. Alloys and Compounds* **2017**, *703*, 330–336, <https://doi.org/10.1016/j.jallcom.2017.01.311>.
- Zhang, Z.; Ma, Y.; Bu, X.; Wu, Q.; Zusheng Z.; Dong, H.Z.; Wu, X. Facile one-step synthesis of TiO₂/Ag/SnO₂ ternary heterostructures with enhanced visible light photocatalytic activity. *Scientific Reports* **2018**, *8*, 10532, <https://doi.org/10.1038/s41598-018-28832-w>.
- Zeferino, R.S.; Pal, U.; De Anda Reues, M.E.; Rosas, E.R. Indium doping induced defect structure evolution and

photocatalytic activity of hydrothermally grown small SnO₂ nanoparticles. *Advances in Nano Research* **2019**, *7*, 13-24, <https://doi.org/10.12989/anr.2019.7.1.013>.

15. Vattikuti, S.V.P.; Reddy, P.A.K.; Shim, J.; Byon, C. Visible-Light-Driven Photocatalytic Activity of SnO₂-ZnO Quantum Dots anchored on g-C₃N₄ nanosheets for photocatalytic pollutant degradation and H₂ production. *ACS Omega* **2018**, *3*, 7587-7602, <https://doi.org/10.1021/acsomega.8b00471>.

16. Zhang, Y.C.; Du, Z.N.; Li, K.W.; Zhang, M.; Dionysiou, D.D. High-Performance Visible-Light-Driven SnS₂/SnO₂ Nanocomposite Photocatalyst Prepared via In situ Hydrothermal Oxidation of SnS₂ Nanoparticles. *ACS Appl. Mater. Interfaces* **2011**, *351*: 528-1537, <https://doi.org/10.1021/am200102y>.

17. Yin, R.; Luo, Q.; Wang, D.; Sun, H.; Li, Y.; Li, X.; An, J. SnO₂/g-C₃N₄ photocatalyst with enhanced visible-light photocatalytic activity. *Journal of Materials Science* **2014**, *49*, 6067-6073.

18. Gao, W.; Zhao, Y.; Mao, Z.; Bi, D.; Chen, J.; Wang, D. Enhanced visible light photocatalytic activity for g-C₃N₄/SnO₂:Sb composites induced by Sb doping. *Journal of Materials Science* **2018**, *13*, <https://doi.org/10.1007/s10853-018-2259-7>.

19. Jiang, X.; Gao, Y.; Li, C.; You, F.; Yao, J.; Ji, Y.; Zhang, Y.; Yao, C. Preparation of hollow yttrium-doped TiO₂ microspheres with enhanced visible-light photocatalytic activity. *Mater. Res. Express* **2019**, *6*, 65510.

20. Wang, J.; Xu, Y.; Xu, W.; Zhang, M.; Chen, X. Simplified preparation of SnO₂ inverse opal form ethanol gas sensing performance. *Microporous Mesoporous Mater.* **2015**, *208*, 93-97, <https://doi.org/10.1016/j.micromeso.2015.01.038>.

21. Zamand, N.; Pour, A.N.; Housaindokth, M.R.; Izadyar, M. Size-controlled synthesis of SnO₂ nanoparticles using reverse microemulsion method. *Solid State Sci.* **2014**, *33*, 6-11, <https://doi.org/10.1016/j.solidstatesciences.2014.04.005>.

22. Chu, G.; Zeng, Q.; Shen, Z.; Zou, H.; Chen, J. Preparation of SnO₂ nanoparticles using ahelical tube reactor via continuous hydrothermal method. *Chem. Eng. J.* **2014**, *253*, 78-83, <http://dx.doi.org/10.1016/j.cej.2014.05.016>.

23. Agrahari, V.; Mathpal, M.C.; Kumar, M.; Agarwal, A. Investigations of optical properties in DMS SnO₂ nanoparticles. *J. Alloys Compd.* **2015**, *622*, 48-53, <https://doi.org/10.1016/j.jallcom.2014.10.009>.

24. Bhattacharjee, A.; Ahmaruzzaman, M.; Sinha, T. A novel approach for the synthesis of SnO₂ nanoparticles and its application as a catalyst in the reduction and photodegradation of organic compounds. *Spectrochim. Acta A* **2015**, *136*, 751-760, <https://doi.org/10.1016/j.saa.2014.09.092>.

25. Soltan, W.B.; Mbarki, M.; Ammar, S.; Babot, O.; Toupance, T. Textural, electrical and optical properties of SnO₂ nanoparticles prepared by polyol method. *J. Mater. Sci. Mater. Electron.* **2015**, *26*, 1612-1628, <https://doi.org/10.1007/s10854-014-2584-9>.

26. Vidhu, V.K.; Philip, D. Biogenic synthesis of SnO₂ nanoparticles: evaluation of antibacterial and antioxidant. *Spectrochim. Acta A* **2015**, *134*, 372-379, <https://doi.org/10.1016/j.saa.2014.06.131>.

27. Shang, G.; Wu, J.; Huang, M.; Lin, J.; Lan, Z.; Huang, Y. Leqing, facile synthesis of mesoporous tin oxide spheres and their applications in dye-sensitized solar cells. *J. Phys. Chem. C* **2012**, *116*, 20140-20145, <https://doi.org/10.1021/jp304185q>.

28. Dattoli, E.N.; Wan, Q.; Guo, W.; Chen, Y.; Pan, X.; Lu, W. Fully transparent thin film transistor device based on SnO₂ nanowires. *Nanowires Nano Lett.* **2007**, *7*, 2463-2469, <https://doi.org/10.1021/nl0712217>.

29. Tammina, S.K.; Mandal, B.K. Tyrosine mediated synthesis of SnO₂ nanoparticles and their photocatalytic activity towards Violet 4 BSN dye. *Journal of Molecular Liquids* **2016**, *221*, 415-421, <https://doi.org/10.1016/j.molliq.2016.05.079>.

6. ACKNOWLEDGEMENTS

The authors greatly acknowledge the help of Vellore Institute of Technology, Vellore 632014, India for the platform given to do this research. The authors greatly acknowledge the analytical supports from the sophisticated Instrumental facilities of SAS, Vellore Institute of Technology, Vellore.



© 2019 by the authors. This article is an open access article distributed under the terms and conditions of the Creative Commons Attribution (CC BY) license (<http://creativecommons.org/licenses/by/4.0/>).